



ScienceDirect

Nuclear Instruments and Methods in Physics  
Research Section A: Accelerators,  
Spectrometers, Detectors and Associated  
Equipment

Volume 500, Issues 1–3, 11 March 2003, Pages 144-162

# Detector physics and simulation of resistive plate chambers

Werner Riegler  , [Christian Lippmann](#), [Rob Veenhof](#)

Show more 

 Outline |  Share  Cite

[https://doi.org/10.1016/S0168-9002\(03\)00337-1](https://doi.org/10.1016/S0168-9002(03)00337-1) 

[Get rights and content](#) 

## Abstract

We present a simulation model suited to study efficiency, timing and pulse-height spectra of Resistive Plate Chambers. After discussing the details of primary ionisation, avalanche multiplication, signal induction and frontend electronics, we apply the model to timing RPCs with time resolution down to **50 ps** and trigger RPCs with time resolution of about **1 ns**.

 Previous

Next 

## PACS

07.05.Tp; 29.40.Cs; 29.40.Gx

## Keywords

RPC; Simulation; Signals; Detector physics; Timing; Efficiency

## 1. Introduction

Resistive Plate Chambers, pioneered during the 1980s [1], [2] and developed into Multi Gap Resistive Plate Chambers during the 1990s [3], have become an integral part of present HEP experiments. A detailed study of signal induction and signal propagation in RPCs can be found in [4], [5]. In this report we focus on the detector physics of RPCs, especially the primary ionisation and avalanche statistics. We present analytical formulae for average signals, charges, time resolution and efficiency to study the ‘order of magnitude’ behaviour of RPCs. We describe a simple Monte Carlo procedure that enables us to simulate accurately the detector physics processes. Effects of high fields, like the change in avalanche statistics and space-charge effects, are also discussed and analysed.

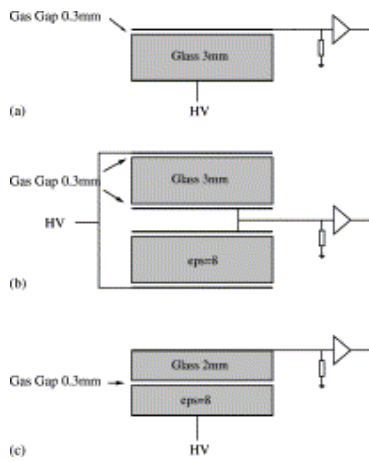
Primary ionisation in gases and avalanche multiplication in a homogeneous electric field were extensively studied already a long time ago. Comprehensive summaries of these topics are given, e.g. in Ref. [6], by R  ther [7], Sauli [8], and, Blum and Rolandi [9]. References to specific publications will be given in the corresponding sections.

Simulation of RPCs was already reported by several authors [10], [11], [12], [13]. The motivation of our work lies in the fact that there are still disagreements about the explanation for several aspects of RPC performance [14]. The high efficiency of single gap RPCs would require a very large ionisation density of the used gases, which according to some authors contradicts experimental values [12], [13]. Even in case the large ionisation density was correct the gas gain has to be extremely large in order to arrive at the observed RPC efficiency, which raises other questions: a very ‘strong’ space-charge effect is required to explain the observed small charges around **1 pC** [15], and doubts have been raised whether an avalanche can progress under such extreme conditions without developing into a forward streamer [13]. To overcome these difficulties, ‘more complex schemes than believed’ like ‘electron extractions from the cathode, or photoionisation in the gas’ were quoted to be very likely [9].

We prefer a scenario where no unusual effects have to be considered, in order to explain the behaviour of RPCs, mainly because the careful simulation of the space-charge effect showed that the required space-charge suppression is indeed possible without streamer effects [16]. In our opinion the detector physics of RPCs does not deviate from the well-known processes that will be discussed throughout this paper.

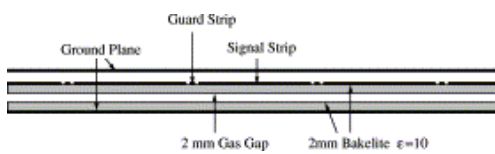
Experimental values for properties of the used RPC gases are scarce. We therefore use values predicted by the widely used programs [17], [18], [19] and perform a RPC simulation based entirely on ‘standard’ detector physics and simulated values for gas properties, without any additional assumptions.

To compare the simulation to measurements we show the results for two different kinds of devices. First we will investigate timing RPCs with a **300  $\mu\text{m}$**  gap, similar to the one developed by Fonte et al. [20], [21], [22] with time resolutions down to **50 ps** (Fig. 1). Similar geometries with **250  $\mu\text{m}$**  gap are described in Ref. [23]. Then we will study **2 mm** gap RPCs similar to the ones in ATLAS [24], [25] with a time resolution of  $\approx$ **1 ns**, used for triggering the experiment (Fig. 2). Both RPC types operate with a gas mixture of  $\text{C}_2\text{F}_4\text{H}_2/\text{i-C}_4\text{H}_{10}/\text{SF}_6$  [26].



[Download: Download full-size image](#)

Fig. 1. RPC geometries similar to the ones developed by Fonte et al. [20], [21], [22].



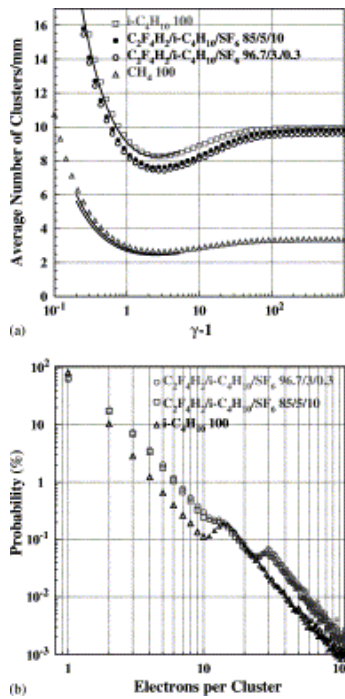
[Download: Download full-size image](#)

Fig. 2. RPC geometry similar to the one used for ATLAS [25].

The timing RPCs by Fonte et al. use gas gaps of  $300\ \mu\text{m}$  and resistive glass plates with a volume resistivity of about  $2 \times 10^{12}\ \Omega\text{cm}$ . The gas is  $\text{C}_2\text{F}_4\text{H}_2/\text{i-C}_4\text{H}_{10}/\text{SF}_6$  85/5/10 at an operating voltage of  $6(3)\ \text{kV}$  for the double(single) gap RPCs, resulting in an electric field of about  $100\ \text{kV/cm}$  in the gas gaps. The ATLAS RPCs use  $2\ \text{mm}$  Bakelite with a volume resistivity of  $9 \times 10^9\ \Omega\text{cm}$ . The  $2\ \text{mm}$  gas gap is filled with  $\text{C}_2\text{F}_4\text{H}_2/\text{i-C}_4\text{H}_{10}/\text{SF}_6$  96.7/3/0.3. The working point is around  $10\ \text{kV}$  giving an electric field of  $50\ \text{kV/cm}$  in the gas gap.

## 2. Primary ionisation

The charge deposit is characterised by the average number of clusters per unit length and the probability distribution for the number of electrons per cluster [9]. The numbers are calculated using Heed [17]. The average number of clusters/mm versus  $(\gamma-1)$  of the particle is shown in Fig. 3(a). For the RPC gas we find an average of 7.5 clusters/mm for a minimum ionising particle. The predicted numbers of isobutane and methane are shown as a reference since measurements for the gases are available [9], [27]. The prediction from Heed of  $8.85\ \text{cl/mm}$  (isobutane) and  $2.64\ \text{cl/mm}$  (methane) for minimum ionising particles matches these specific experimental results very well. It has to be mentioned that other experimental values quoted in literature are considerably lower than these, e.g. [8]  $4.6\ \text{cl/mm}$  (isobutane) and  $1.6\ \text{cl/mm}$  (methane). We prefer the high values since they were obtained with a very careful setup [27], they are well reproduced by Heed [17] and they resolve the RPC puzzles mentioned in the introduction.



[Download: Download full-size image](#)

Fig. 3. (a) Average number of clusters/mm for different gases at **296.15 K** and **1013 mbar** as predicted by Heed [17]. The solid lines show measurements for methane and isobutane from Ref. [27]. (b) Cluster size distribution for a **7 GeV** pion (isobutane and 10%  $SF_6$  mixture) and **120 GeV** muon (0.3%  $SF_6$  mixture) as simulated by Heed. Cutting at 500 electrons the average number of electrons/cluster is 1.9 for isobutane, 2.6 for the 10%  $SF_6$  mixture and 2.8 for the 0.3%  $SF_6$  mixture.

For the RPC gas and a **7 GeV** pion, we find on average **9.5 clusters/mm**, so the average distance between clusters is  $\lambda=105 \mu\text{m}$ . The cluster size distribution for three gases is shown in Fig. 3(b). For the simulation of wire chambers [28], omitting the long tail in the cluster size distribution can give results that are in sharp disagreement with observation. One therefore has to carefully set the cut in the distribution according to detector under consideration. E.g. for the  $C_2F_4H_2/i-C_4H_{10}/SF_6$  96.7/3/0.3 gas, the probability for a cluster to contain more than 30 electrons is 1%. Therefore, the probability that at least one of the  $\approx 20$  primary clusters in a **2 mm** RPC contains more than 30 electrons is still 20%. To be ‘safe’ from any error due to this cut, and because it does not require much CPU time, the cut was set to 500 electrons in the simulations presented throughout this paper. The distance between the clusters is exponentially distributed, so the probability to find the first cluster between position  $x$  and  $x+dx$  is [9]

$$P(x)=1\lambda e^{-x/\lambda} \quad (1)$$

The probability for the  $n$ th cluster to be between position  $x$  and  $x+dx$ , independent of the position of all the others, is given by [8]

$$P_{clu}(n,x)=f_0x f_0x_{n-1} \dots f_0x_2 P(x_1)P(x_2-x_1)P(x-x_{n-1}) dx_1 dx_2 \dots dx_{n-1} = x^{n-1} (n-1)! \lambda^n e^{-x/\lambda} \quad (\Gamma \text{ distribution}) \quad (2)$$

with an average distance from the gas gap edge of  $\bar{x}=n\lambda$ . For the simulation we simply put the primary clusters with relative distances according to Eq. (1) and the number of electrons for each cluster from the cluster size distribution in Fig. 3b.

### 3. Secondary particles

Secondary particles created by the incident particle in the RPC material potentially have a very big impact on the RPC performance since these particles, mostly delta electrons, create many ionisation electrons at the ‘beginning’ of the gas gap. For the RPCs in Fig. 1(a) and (b), the particle enters the gas gap through an aluminium plate. A calculation with Fluka [29], [30] for a 7 GeV pion crossing a 3 mm aluminium plate shows that the probability that the pion is accompanied by at least one charged particle is only 4.92%. Therefore, the secondaries should not have a serious influence on the charge spectrum, efficiency and timing.

### 4. Avalanche multiplication

Each electron will start an avalanche which will grow until it hits the resistive plate or metal electrode. Avalanche multiplication for electronegative gases at high fields is described in detail in Ref. [31]. In case the probability that an electron multiplies is independent of the previous position of multiplication, the avalanche development is characterised by the Townsend coefficient  $\alpha$  and attachment coefficient  $\eta$ . Fig. 4 shows these parameters as calculated with Imonte [19]. For the trigger RPCs with  $E=50\text{ kV/cm}$  we expect an effective Townsend coefficient of around 10/mm while for the timing RPCs with  $E=100\text{ kV/cm}$  we expect a value around 113/mm. If the avalanche contains  $n$  electrons at position  $x$  the probability that it contains  $n+1$  at  $x+dx$  is given by  $n\alpha dx$ . Following the same arguments, the probability that for an avalanche of size  $n$ , one electron gets attached (forming a negative ion) over distance  $dx$ , is  $n\eta dx$ . For the average number of electrons  $\bar{n}$  and positive ions  $\bar{p}$  we therefore have the relations [7], [31]

$$d\bar{n}dx=(\alpha-\eta)\bar{n}, d\bar{p}dx=\alpha\bar{n} \quad (3)$$

with  $\bar{n}(0)=1$  and  $\bar{p}(0)=0$  giving the solution [7], [31]

$$\bar{n}(x)=e^{(\alpha-\eta)x}, \bar{p}(x)=\alpha\alpha-\eta(e^{(\alpha-\eta)x}-1). \quad (4)$$

The average number of negative ions is then  $\bar{p}-\bar{n}$ . To derive the statistical fluctuation of the avalanche, we proceed as shown in Ref. [31]. The probability  $P(n,x)$  for an avalanche started with a single electron to contain  $n$  electrons after distance  $x$  is defined by

$$P(n,x+dx)=P(n-1,x)(n-1)\alpha dx(1-(n-1)\eta dx)+P(n,x)(1-n\alpha dx)(1-n\eta dx)+P(n,x)n\alpha dx n\eta dx+P(n+1,x)(1-(n+1)\alpha dx)(n+1)\eta dx. \quad (5)$$

The four lines represent the four possibilities to find  $n$  electrons at position  $x+dx$ . The first line gives the probability that there are  $n-1$  electrons at  $x$ , exactly one of them duplicates and no electron is attached. The second line gives the probability that there are  $n$  electrons at  $x$ , no electron duplicates and no electron is attached. The third line gives the probability that from  $n$  electrons, one multiplies and one gets attached and finally the fourth line gives the probability that from  $n+1$  electrons one gets attached and no electron is multiplied. Evaluating the expression and omitting the higher order terms of  $dx$  we find

$$dP(n,x)dx=-P(n,x)n(\alpha+\eta)+P(n-1,x)(n-1)\alpha+P(n+1,x)(n+1)\eta \quad (6)$$

with the general solution [31]

$$P(n,x)=k\bar{n}(x)-1\bar{n}(x)-k,n=0\bar{n}(x)(1-k\bar{n}(x)-k)^2(\bar{n}(x)-1\bar{n}(x)-k)^{n-1}, n>0 \quad (7)$$

where

$$\bar{n}(\mathbf{x}) = e^{(\alpha - \eta)\mathbf{x}}, \mathbf{k} = \eta\alpha. \quad (8)$$

The variance  $\sigma^2(x)$  of the distribution is given by

$$\sigma^2(\mathbf{x}) = 1 + \mathbf{k} - \mathbf{k}\bar{n}(\mathbf{x})(\bar{n}(\mathbf{x}) - 1). \quad (9)$$

We see that the average electron number depends on the so-called effective Townsend coefficient  $\alpha_{\text{eff}} = \alpha - \eta$ , the variance and the distribution itself however depends also on  $k = \eta/\alpha$  explicitly. For illustration, Fig. 5 shows the above distribution for the same effective Townsend coefficient but different  $\alpha$  and  $\eta$ . For simulation of avalanche fluctuations, the Furry law and the Polya distribution [32] are widely used. Both of them do not contain the effect of attachment which has a significant influence on the charge spectrum as seen from Fig. 5. They are therefore not applicable for the avalanche fluctuations in RPC gases which show strong attachment. For a distance  $x$  where  $\bar{n}$  is sufficiently large, we can approximate the above formula and find [31]

$$P(\mathbf{n}, \mathbf{x}) = \mathbf{k}, \mathbf{n} = 0 (1 - \mathbf{k})^2 \bar{n}(\mathbf{x}) \exp[-(1 - \mathbf{k})\mathbf{n}\bar{n}(\mathbf{x})], \mathbf{n} > 0. \quad (10)$$

In the case that  $\alpha = \eta$  or 0 the distribution from Eq. (7) becomes undefined and we have to use different expressions. These cases are important when the space-charge effects are taken into account [16]. In case  $\alpha = \eta$  the probabilities are

$$P(\mathbf{n}, \mathbf{x}) = \alpha \mathbf{x}^{1 + \alpha \mathbf{x}}, \mathbf{n} = 0 (1 + \alpha \mathbf{x})^2 (\alpha \mathbf{x}^{1 + \alpha \mathbf{x}})^{\mathbf{n} - 1}, \mathbf{n} > 0 \quad (11)$$

and the variance becomes

$$\sigma^2(\mathbf{x}) = 2\alpha \mathbf{x}. \quad (12)$$

In case  $\alpha = 0$  the probabilities are

$$P(\mathbf{n}, \mathbf{x}) = 1 - e^{-\eta \mathbf{x}}, \mathbf{n} = 0 e^{-\eta \mathbf{x}}, \mathbf{n} = 1 \quad (13)$$

and the probability to find  $n > 1$  electrons is zero. The variance is

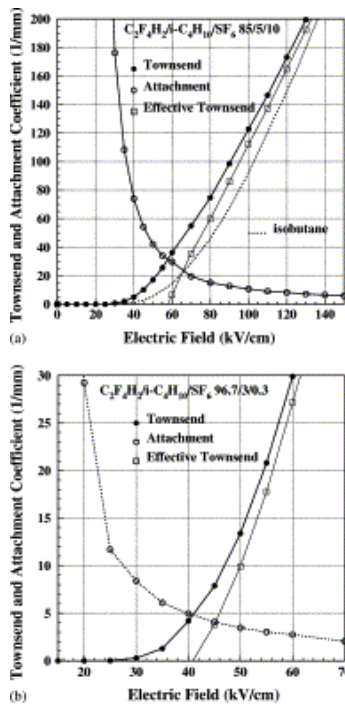
$$\sigma^2(\mathbf{x}) = e^{-2\eta \mathbf{x}} (e^{\eta \mathbf{x}} - 1). \quad (14)$$

To generate a random number according to Eq. (7) one draws a uniform random number  $s$  from the interval (0,1) and calculates

$$\mathbf{n}0, s < \mathbf{k}\bar{n}(\mathbf{x}) - 1 \bar{n}(\mathbf{x}) - \mathbf{k} 1 + \text{Trunc}[1 \ln(1 - 1 - \mathbf{k}\bar{n}(\mathbf{x}) - \mathbf{k}) \ln((\bar{n}(\mathbf{x}) - \mathbf{k})(1 - s)\bar{n}(\mathbf{x})(1 - \mathbf{k}))], s > \mathbf{k}\bar{n}(\mathbf{x}) - 1 \bar{n}(\mathbf{x}) - \mathbf{k} \quad (15)$$

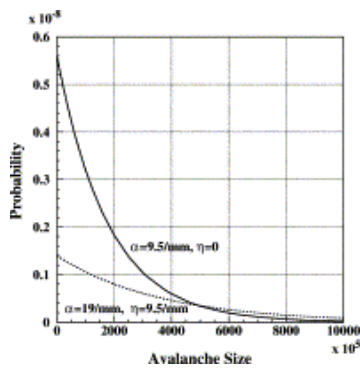
where ‘Trunc’ means truncation of the decimals. In case  $\bar{n}(\mathbf{x})$  is very large the numerical evaluation of the first factor can become problematic and it is better to use the series expansion for

$$\ln(1 - \mathbf{x}) = -(\mathbf{x} + \frac{1}{2}\mathbf{x}^2 + \frac{1}{3}\mathbf{x}^3 + \dots).$$



Download: [Download full-size image](#)

Fig. 4. Townsend and attachment coefficient as calculated by Imonte [19] for  $T=296.15\text{K}$  and  $P=1013\text{mbar}$  for the timing RPC (a) and trigger RPC (b) gas.



Download: [Download full-size image](#)

Fig. 5. Charge distribution for avalanches starting with a single electron. The effective Townsend coefficient  $\alpha-\eta$  is the same for both curves.

To generate a random number according to Eq. (11) one draws a uniform random number  $s$  from the interval  $(0,1)$  and calculates

$$n=0, s < \alpha x_1 + \alpha x_1 + \text{Trunc}[1 \ln(\alpha x_1 + \alpha x) \ln((1-s)(1+\alpha x))], s > \alpha x_1 + \alpha x. \quad (16)$$

To generate a random number according to Eq. (13) one calculates

$$n=0, s > e^{-\eta x} 1, s < e^{-\eta x}. \quad (17)$$

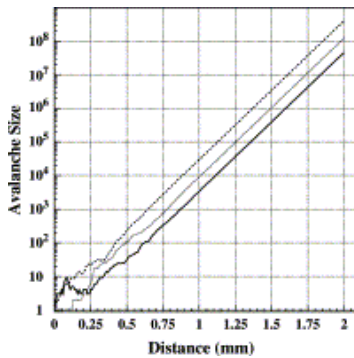
If we want to calculate the induced signal, we have to simulate the avalanche development instead of using the probability distribution for the final avalanche charge. Let us first follow the avalanche development for a single initial electron starting at one edge of the gas gap. We divide the gap into  $N$  steps of  $\Delta x$ . The average multiplication  $\bar{n}(\Delta x)$  for a single electron over this distance is given by  $e^{(\alpha-\eta)\Delta x}$ .



Starting with one electron at  $x=0$  we find  $n_1$  electrons at  $x=\Delta x$  where  $n_1$  is from , , . Each of these electrons will again multiply the same way. To find the number  $n_2$  of electrons at  $x=2\Delta x$ , we loop over the  $n_1$  electrons, draw a number from , , for each electron and sum them. This procedure can be repeated through the full gap, but it is very time consuming. If the number of electrons  $n_i$  at a given distance of  $i\Delta x$  is sufficiently large, we can use the central limit theorem and calculate the number of electrons  $n_{i+1}$  at distance  $(i+1)\Delta x$  by drawing a random number from a Gaussian with mean  $\mu$  and sigma  $\sigma_\mu$  of

$$\mu=n_i\bar{n}(\Delta x),\sigma_\mu=n_i\sigma(\Delta x) \quad (18)$$

where  $\sigma(x)$  is from , and (14). This makes the simulation procedure very fast. Fig. 6 shows examples of individual avalanches starting from a single electron. The very beginning of the avalanche decides on the final avalanche size. Once the number of electrons has reached a certain size the avalanche grows smoothly like  $e^{(\alpha-\eta)x}$ .



[Download: Download full-size image](#)

Fig. 6. Avalanches started by a single electron at  $x=0$  for  $\alpha=13/\text{mm}, \eta=3.5/\text{mm}$ . We see that the very beginning of the avalanche decides on the final avalanche size. Once the number of electrons is sufficiently large the avalanche grows like  $e^{(\alpha-\eta)x}$ .

## 5. Induced signals

The movement of the electrons in the electric field finally induces a current signal on the RPC electrodes. The negative and positive ions induce a signal which is much smaller due to their slow drift velocity which we will neglect in the following. Fig. 7 shows the drift velocities for different gases as predicted by Magboltz [18] together with some measurements. The current signal induced on an electrode is given by [35], [7]

$$\mathbf{i}(t)=\mathbf{E}_w \cdot \mathbf{v} V_w e_0 N(t) \quad (19)$$

where  $e_0$  is the electron charge,  $E_w$  (weighting field) is the electric field in the gas gap if we put the electrode to potential  $V_w$  and ground all other electrodes,  $v$  is the electron drift velocity and  $N(t)$  is the number of electrons present at time  $t$  which we calculate by simulating the avalanches of the individual primary electrons. The weighting fields  $E_w/V_w$  for the geometries in Fig. 1, Fig. 2 (considering the electrodes to be large compared to the RPC thickness) can be calculated the following way: the electric fields  $E_i$  in a capacitor with  $n$  layers of thickness  $d_i$  and permittivity  $\epsilon_i$  can be calculated by the conditions

$$\sum \mathbf{i}=1 \mathbf{n} E_i d_i=V_w, \epsilon_i E_i=\epsilon_j E_j \text{ for neighbouring layers.} \quad (20)$$

For geometries (a), (b), (c) of Fig. 1 we therefore have



$$E_w V_w = \varepsilon_r b + d \varepsilon_r \quad (21a)$$

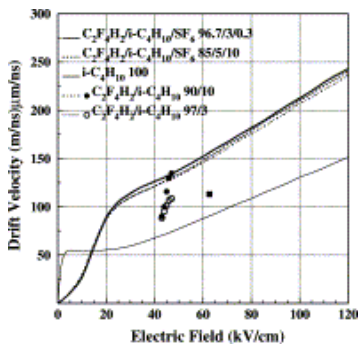
$$E_w V_w = \varepsilon_r b + 2d \varepsilon_r \quad (21b)$$

$$E_w V_w = \varepsilon_r 2b + d \varepsilon_r \quad (21c)$$

where  $\varepsilon_r$  is the Bakelite (glass) permittivity,  $b$  the Bakelite (glass) thickness and  $d$  the gas gap. To get an idea about the signals we first assume a single primary electron somewhere in the gas gap. Using the result that after some initial fluctuations  $N(t)$  grows like a smooth exponential (Fig. 6) and that the charge after a fixed distance (time) is exponentially distributed (Eq. (10)), we can assume an RPC signal distribution of

$$i(t) = A e^{(\alpha - \eta)vt}, P(A) = 1 A_{av} e^{-A/A_{av}} \quad (22)$$

where  $P(A)$  is the probability to find the amplitude  $A$  in an event. This signal growth distribution is independent of the position of the primary electron in the gas gap. The position only determines when the avalanche hits the electrode, i.e. it determines when the signal is stopped.



Download: [Download full-size image](#)

Fig. 7. The lines show the drift velocity for different gases at **296.15 K** and **1013 mbar** as predicted by Magboltz [18]. The circles show measurements from Ref. [33], the solid square shows a measurement for  $C_2F_4H_2/i-C_4H_{10}/SF_6$  96.9/3/0.1 from Ref. [34].

If the gas gap is large compared to the average distance between clusters, the signal is formed by many clusters. To get an idea of the average pulse height and signal shape, we assume  $N_0 = d/\lambda$  clusters distributed evenly in the gas gap, each containing  $n_{av}$  electrons ( $d$  is the gap thickness and  $\lambda$  is the average distance between clusters). The signal is then given by

$$I(t) = E_w V_w e_0 v N(t),$$

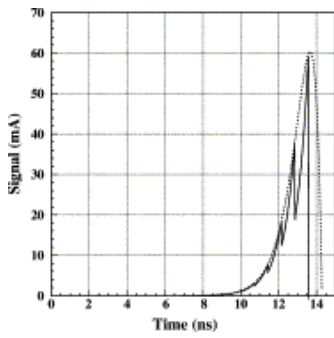
$$N(t) = \sum_{n=1}^{N_0} n N_0 n_{av} e^{(\alpha - \eta)vt} \Theta(dv - nN_0 - t) \quad (23)$$

where  $\Theta(x)$  is the step function. The enveloping function of this signal is

$$I_{env}(t) = E_w V_w e_0 v N_{env}(t),$$

$$N_{env}(t) = N_0 n_{av} 1 - tv d e^{(\alpha - \eta)vt} \Theta(dv - t). \quad (24)$$

Both of these functions are shown in Fig. 8. These formulas only match to reality if saturation effects can be neglected.



Download: [Download full-size image](#)

Fig. 8. Average signal from Eq. (23) with the enveloping function from Eq. (24) for the Trigger RPC geometry with parameters from Eq. (26).

To discuss the performance numbers in the next sections we use the parameters from the previous figures at typical operating voltages:

$$\text{Timing RPC: } E=100 \text{ kV/cm}, \alpha=123/\text{mm}, \eta=10.5/\text{mmv}=210 \mu\text{m/ns}, d=0.3 \text{ mm}, \epsilon_r=8\lambda=0.1 \text{ mm}, n_{av}=2.6, b=2 \text{ mm}. \quad (25)$$

$$\text{Trigger RPC: } E=50 \text{ kV/cm}, \alpha=13.3/\text{mm}, \eta=3.5/\text{mmv}=140 \mu\text{m/ns}, d=2 \text{ mm}, \epsilon_r=10\lambda=0.1 \text{ mm}, n_{av}=2.8, b=2 \text{ mm} \quad (26)$$

where  $\alpha$  is the Townsend coefficient,  $\eta$  the attachment coefficient,  $d$  the gas gap,  $\epsilon_r$  the Bakelite (glass) permittivity,  $\lambda$  the average distance between clusters,  $n_{av}$  the average number of electrons per cluster,  $b$  the Bakelite (glass) thickness and  $v$  the electron drift velocity.

## 6. Average signals and charges

In the following we will derive analytic expressions for the average signal and charge produced by the individual clusters as well as the total charge deposit. Comparing these formulas to measurements will show the importance of saturation effects in RPCs. We will frequently use the integral

$$\int_0^R x^n e^{-x} dx = n!(1 - K[R, n+1]) \text{ with } K[R, n] = e^{-R} \sum_{k=0}^{n-1} \frac{R^k}{k!}. \quad (27)$$

### 6.1. Individual clusters

Using  $P_{clu}$  from Eq. (2), the average number of electrons  $N_n^-$  produced by the  $n$ th cluster is given by

$$N_n^- = \int_0^d P_{clu}(n, x) n_{av} \bar{n}(d-x) dx = n_{av} e^{(\alpha-\eta)d} [1 + (\alpha-\eta)\lambda]^n - K d \alpha - \eta + 1 \lambda, n \approx n_{av} e^{(\alpha-\eta)d} [1 + (\alpha-\eta)\lambda]^n \text{ for } e^{(\alpha-\eta)d} \gg 1. \quad (28)$$

The average number of positive ions  $N_n^+$  produced by the  $n$ th cluster is

$$N_n^+ = \int_0^d P_{clu}(n, x) n_{av} \bar{p}(d-x) dx = n_{av} \alpha \lambda e^{(\alpha-\eta)d} [1 + (\alpha-\eta)\lambda]^n - K d \alpha - \eta + 1 \lambda, n - 1 - K d \lambda, n \approx n_{av} e^{(\alpha-\eta)d} (\alpha-\eta) [1 + (\alpha-\eta)\lambda]^n \text{ for } e^{(\alpha-\eta)d} \gg 1. \quad (29)$$

The average signal from a single electron starting at position  $x$  in the RPC gap is

$$i(t, x) = E_w V_w e_0 v e^{(\alpha-\eta)vt} \Theta(d-xv-t) \quad (30)$$

and the corresponding induced charge is

$$Q_n^{\text{ind}}(d-x) = \int_0^\infty \int \mathbf{i}(t, \mathbf{x}) dt = E_w \epsilon_0 V_w (\alpha - \eta) (e^{(\alpha - \eta)(d-x)} - 1) = E_w V_w 1 \alpha \bar{p}(d-x). \quad (31)$$

Therefore the average charge  $Q_n^{\text{ind}}$  induced by the  $n$ th cluster is

$$Q_n^{\text{ind}} = \int_0^d P_{\text{clu}}(n, \mathbf{x}) n_{\text{av}} Q_n^{\text{ind}}(d-x) d\mathbf{x} = E_w \epsilon_0 V_w 1 \alpha N_n^+ \quad (32)$$

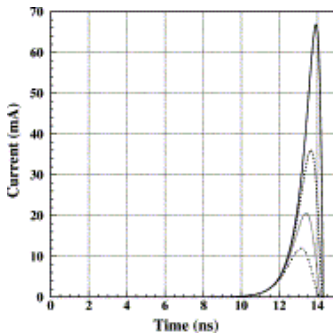
and hence the ratio of induced charge and ion charge, which is equal to the total avalanche charge, measures the Townsend coefficient independent of attachment [36]:

$$Q_n^{\text{ind}} / Q_{\text{avalanche } n} = E_w V_w 1 \alpha. \quad (33)$$

The average signal due to the  $n$ th cluster is given by

$$\bar{i}_n(t) = \int_0^d P_{\text{clu}}(n, \mathbf{x}) n_{\text{av}} \mathbf{i}(t, \mathbf{x}) d\mathbf{x} = E_w V_w \epsilon_0 v n_{\text{av}} e^{(\alpha - \eta)t} [1 - K 1 \lambda (d - vt)] n \Theta dv - t. \quad (34)$$

The average signals of the first four clusters for the parameters from Eq. (26) are shown in Fig. 9.



[Download: Download full-size image](#)

Fig. 9. Average signals from the first four clusters for the parameters from Eq. (26).

## 6.2. All clusters

In this section we calculate the average total charge and signal. The distance between the individual clusters is exponentially distributed

$$P(\Delta \mathbf{x}) = 1 \lambda e^{-\Delta \mathbf{x} / \lambda}. \quad (35)$$

Therefore the probability to have the first cluster at position  $x_1$ , the second one at position  $x_2 > x_1$ , ..., the  $n$ th cluster at position  $x_n > x_{n-1}$  and no other cluster in the gas gap  $x_{n+1} > d$  is given by

$$\int d\mathbf{x} P(\mathbf{x}_1) P(\mathbf{x}_2 - \mathbf{x}_1) \cdots P(\mathbf{x}_{n+1} - \mathbf{x}_n) d\mathbf{x}_{n+1} = 1 \lambda^n e^{-d/\lambda}. \quad (36)$$

The probability to have exactly  $n$  electrons in the gas gap, independent of position, is given by the integral over all positions

$$\int_0^d \int_0^{\mathbf{x}_n} \int_0^{\mathbf{x}_{n-1}} \cdots \int_0^{\mathbf{x}_2} 1 \lambda^n e^{-d/\lambda} d\mathbf{x}_1 d\mathbf{x}_2 \cdots d\mathbf{x}_n = 1 n! d \lambda^n e^{-d/\lambda} \quad (37)$$

which is the expected Poisson distribution [9]. The average number of avalanche electrons  $N^-$  is given by

$$\begin{aligned} \mathbf{N}^- &= \sum_{\mathbf{n}=1}^{\infty} \int_0^d \int_0^{x_n} \int_0^{x_{n-1}} \dots \int_0^{x_2} 1 \lambda^n e^{-d/\lambda} n_{\text{av}} [\bar{n}(d-x_1) + \bar{n}(d-x_2) + \dots + \bar{n}(d-x_n)] dx_1 dx_2 \dots dx_n = \sum_{\mathbf{n}=1}^{\infty} \int_0^d \int_0^{x_n} \int_0^{x_{n-1}} \dots \int_0^{x_2} 1 \lambda^n e^{-d/\lambda} n_{\text{av}} (e^{(\alpha-\eta)d} - 1) d^{n-1} e^{-d/\lambda} (n-1)! (\alpha-\eta) \lambda^n = n_{\text{av}} \lambda (\alpha-\eta) (e^{(\alpha-\eta)d} - 1) \approx n_{\text{av}} e^{(\alpha-\eta)d} \lambda (\alpha-\eta) \text{ for } e^{(\alpha-\eta)d} \gg 1. \end{aligned} \quad (38)$$

The average number of ions  $\mathbf{N}^+$  is derived by replacing  $\bar{n}(d-x_n)$  by  $\bar{p}(d-x_n)$  in the above expression and we find

$$\mathbf{N}^+ = n_{\text{av}} \alpha (\alpha - \eta) \lambda (e^{(\alpha-\eta)d} - 1) \approx n_{\text{av}} \alpha \lambda (\alpha - \eta)^2 e^{(\alpha-\eta)d} \text{ for } e^{(\alpha-\eta)d} \gg 1. \quad (39)$$

The average induced charge  $\mathbf{Q}_{\text{ind}}$  is as before proportional to the number of ions

$$\mathbf{Q}_{\text{ind}} = E_w V_w e_0 \alpha \mathbf{N}^+ \approx E_w V_w n_{\text{av}} e_0 \lambda (\alpha - \eta)^2 e^{(\alpha-\eta)d} \text{ for } e^{(\alpha-\eta)d} \gg 1. \quad (40)$$

The average RPC Signal is given by

$$\begin{aligned} \bar{i}(t) &= \sum_{\mathbf{n}=1}^{\infty} \int_0^d \int_0^{x_n} \int_0^{x_{n-1}} \dots \int_0^{x_2} 1 \lambda^n e^{-d/\lambda} [i(t, x_1) + i(t, x_2) + \dots + i(t, x_n)] dx_1 dx_2 \dots dx_n = \sum_{\mathbf{n}=1}^{\infty} \int_0^d \int_0^{x_n} \int_0^{x_{n-1}} \dots \int_0^{x_2} 1 \lambda^n e^{-d/\lambda} E_w V_w n_{\text{av}} e_0 v e^{(\alpha-\eta)t} \sum_{\mathbf{k}=1}^{\mathbf{n}} \Theta(d - x_n - v - t) dx_1 dx_2 \dots dx_n = \sum_{\mathbf{n}=1}^{\infty} \int_0^d \int_0^{x_n} \int_0^{x_{n-1}} \dots \int_0^{x_2} 1 \lambda^n e^{-d/\lambda} (d - vt) \Theta(d - vt) dv - t. \end{aligned} \quad (41)$$

We find that the average RPC signal is equal to the enveloping function from Eq. (24).

## 7. Intrinsic timing

In this section we want to find an order of magnitude formula for the intrinsic timing of a single gap RPC. Details on this can be found in Ref. [37]. For sufficiently low thresholds (and fast amplifiers), the timing is not affected by saturation effects. We assume a single primary electron somewhere in the RPC. The RPC signal and amplitude fluctuation is then given by Eq. (22). Setting a threshold of  $A_{\text{thr}}$  to the RPC signal we find a threshold crossing time of

$$\begin{aligned} i(t) &= A e^{(\alpha-\eta)vt} = A_{\text{thr}} \rightarrow \\ t(A) &= \frac{1}{(\alpha-\eta)v} \ln \frac{A}{A_{\text{thr}}}. \end{aligned} \quad (42)$$

The amplitude  $A$  is exponentially distributed around some average amplitude  $A_{\text{av}}$ . Therefore, the time distribution  $P(t)$  for a given threshold is given by

$$\begin{aligned} P(t) &= \int_0^{\infty} \delta(A - A_{\text{thr}} e^{(\alpha-\eta)vt}) \lambda A_{\text{av}} e^{-\lambda A_{\text{av}}} dA = \lambda A_{\text{thr}} (\alpha-\eta)v e^{-(\alpha-\eta)vt} \exp\left[-(\alpha-\eta)vt \frac{A_{\text{thr}}}{A_{\text{av}}}\right] e^{-\lambda A_{\text{thr}} \frac{A_{\text{av}}}{(\alpha-\eta)v} e^{-(\alpha-\eta)vt}} \end{aligned} \quad (43)$$

where  $\delta(x)$  is the Dirac delta function. This distribution has the curious property that a different threshold merely corresponds to a time shift, i.e. the shape of the distribution is independent of threshold and average amplitude. Time shifting the maximum to zero, the distribution reads

$$P(t) = (\alpha-\eta)v F((\alpha-\eta)vt), F(x) = \exp(-x - \exp(-x)). \quad (44)$$

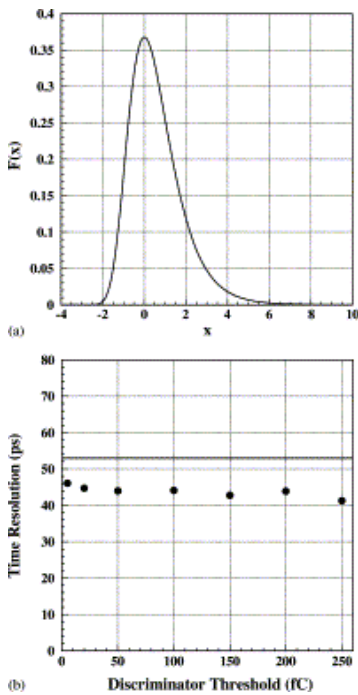
The function is shown in Fig. 10. The variance  $\sigma$  of the function  $F(x)$  is given by

$$\sigma(F) = 1.28 \quad (45)$$

so the RPC time resolution is given by

$$\sigma_t = 1.28(\alpha - \eta)v \quad (46)$$

where  $\alpha - \eta$  is the effective Townsend coefficient and  $v$  is the electron drift velocity. We therefore expect that the intrinsic time resolution depends only on the drift velocity and the effective Townsend coefficient and not on the threshold. This is reproduced by the detailed Monte Carlo simulation (Fig. 10(b)) and also observed in measurements [21].



[Download: Download full-size image](#)

Fig. 10. (a) The function  $F(x)$  from Eq. (45) giving the RPC approximate time resolution. The time resolution scales with  $1/(\alpha - \eta)v$  which just ‘stretches the abscissa’. (b) Full Monte Carlo simulation of the time resolution versus threshold for the  $300 \mu\text{m}$  RPC at  $3 \text{ kV}$  with  $t_p = 0.5 \text{ ns}$  and ENC  $1 \text{ fC}$ . The solid line shows Eq. (47).

For the timing RPC with parameters from Eq. (25)  $\sigma_t \approx 50 \text{ ps}$  and for Trigger RPCs with parameters from Eq. (26) we find  $\sigma_t \approx 1 \text{ ns}$ . These numbers are quite close to the ones quoted in [38], [40]. Intrinsic time resolution of RPCs is therefore dominated by the effective Townsend coefficient and the drift velocity and is to first-order independent of the primary ionisation parameters.

## 8. Efficiency

In this section we want to estimate the efficiencies that we expect with the detector physics model and numbers given before. In a simplified view we expect the RPC to be efficient if the first cluster creates an avalanche that exceeds the threshold or the first cluster is attached and the second cluster exceeds the threshold or the first and second cluster are attached and the third exceeds the threshold, etc. In addition we assume that the clusters contain only one electron and we neglect avalanche fluctuations [12], i.e. a primary electron at position  $x$  in the gas gap will induce a charge of

$$Q_{\text{ind}}(x) = E_w V_w e_0 \alpha - \eta e^{(\alpha - \eta)(d - x)} - 1 \quad (47)$$

on the readout electrode. Setting a threshold of  $Q_t$ , the condition for an efficient event is  $Q_{\text{ind}}(x) > Q_t$  meaning  $x < x_0$  with [12]

$$x_0 = d - 1\alpha - \eta \ln 1 + V_w E_w \alpha - \eta e_0 Q_t. \quad (48)$$

The probability that the first cluster is not attached and above threshold is

$$P_1 = 1 - \eta \alpha \int_0^{x_0} \lambda e^{-x/\lambda} dx. \quad (49)$$

The probability that the first cluster is attached and the second one is not attached and above threshold is

$$P_2 = \int_0^{x_0} \int_0^{x_2} \eta \alpha \lambda e^{-x_1/\lambda} (1 - \eta \alpha \lambda e^{-(x_2 - x_1)/\lambda}) dx_1 dx_2. \quad (50)$$

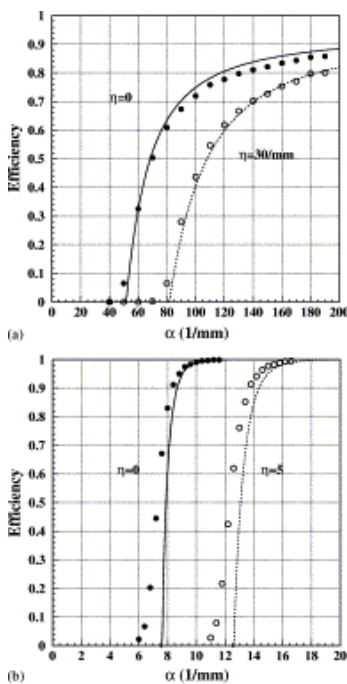
Continuing the series and evaluating the integrals, the probability for the  $n$ th cluster to be above threshold and the  $n-1$  before to be attached is

$$P_n = \eta \alpha^{n-1} (1 - \eta \alpha)^{n-1} K(x_0, \lambda, n) \quad (51)$$

where  $K[x, n]$  is from Eq. (27). The efficiency  $\varepsilon$  is then given by

$$\varepsilon = \sum_{n=1}^{\infty} P_n = 1 - e^{-(1-\eta/\alpha)d/\lambda} (1 + V_w E_w \alpha - \eta e_0 Q_t)^{1/\alpha\lambda}. \quad (52)$$

The efficiency depends explicitly on  $\alpha$  and  $\eta$  and not just on the effective Townsend coefficient. For  $\alpha \rightarrow \infty$  the inefficiency is  $\exp[-d/\lambda]$  which is the probability that there is no primary cluster in the gas gap. This formula together with a full Monte Carlo simulation is shown in Fig. 11. For the **2 mm** RPC, the formula underestimates the efficiency since it does not take into account the possibilities that individual avalanches stay below the threshold but that the sum crosses the threshold. However, the order of magnitude of the efficiency can be estimated quite well.



[Download: Download full-size image](#)

Fig. 11. Efficiency from Eq. (53) together with the full Monte Carlo for a (a) **0.3 mm** RPC and (b) **2 mm** RPC.

## 9. Space-charge effects

Inserting the detector physics parameters from , in , we find average charges that are significantly larger than the measured ones (measurements in brackets)

$$\text{Timing RPC: } Q_{\text{tot}} \approx 1.8 \times 10^7 \text{ (5) pC, } Q_{\text{ind}} \approx 1.9 \times 10^5 \text{ (0.5) pC} \quad \text{Trigger RPC: } Q_{\text{tot}} \approx 200 \text{ (40) pC, } Q_{\text{ind}} \approx 6 \text{ (2) pC.} \quad (53)$$

The discrepancy for the total charge value is a factor  $\approx 5$  for the trigger RPCs and  $\approx 3.4 \times 10^6$  for the timing RPCs! Using Eq. (38) we find the average number of avalanche electrons for the timing RPC to be  $\approx 10^{14}$ . Assuming a single electron avalanche in the timing RPC, the electron cloud will assume a Gaussian shape with  $\sigma \approx 20 \mu\text{m}$  after  $300 \mu\text{m}$  due to longitudinal and transverse diffusion. Assuming a sphere of charge with  $10^6$  electrons and radius of  $20 \mu\text{m}$ , the field on the surface is  $36 \text{ kV/cm}$ , so for numbers of  $10^6 - 10^7$  electrons, the fields in the avalanche become comparable to the applied field. Therefore, space-charge effects must play a significant role in this detector [15]. It is shown in Ref. [16] that taking into account the field of the avalanche correctly explains the observed charges. In this report we take the effect into account in a crude way by allowing the avalanche growth only up to a certain size as proposed in [26], [12]

## 10. Avalanche statistics at high fields

The assumption that the ionisation probability is independent of the history of previous collisions will not hold above a certain electric field value. Considering a Townsend coefficient of  $\alpha = 123/\text{mm}$  at the electric field  $\mathbf{E} = 100 \text{ kV/cm}$ , the average distance between ionising collisions  $1/\alpha$  is  $8.13 \mu\text{m}$ . Assuming an ionisation energy of  $U_i = 25 \text{ eV}$  an electron has to travel a distance of  $x_0 = U_i/E = 2.5 \mu\text{m}$  after a collision to again reach this energy, so within  $2.5 \mu\text{m}$  after each collision the ionisation probability is zero. Since this number is comparable to  $1/\alpha$  the condition that the ionisation probability is independent of the previous collisions does not hold any more and the avalanche fluctuations will be altered. Instead the shape of the distribution depends on the parameter [7]

$$r = 1 + \alpha E U_i. \quad (54)$$

At low fields ( $r \ll 1$ ) the avalanches started by a single electron (and multiplying over a fixed distance) result in the distribution described in the previous chapter. At high fields ( $r \approx 1$ ) the distributions show a pronounced maximum for which many different interpretations were given [41]. A popular way to describe this phenomenon is the Polya distribution which derived from the probability  $p$  to find  $n+1$  electrons in  $x+dx$  as

$$p = n \lambda b - 1 - b n dx. \quad (55)$$

We see that this distribution assumes that the probability to create an electron depends on the current size of the avalanche. This however misses a clear physical interpretation and describes some kind of space-charge effect which we include in the way mentioned above. Therefore the only justification for this distribution is that it can parametrise the measured curves in a nice way.

For this study we will, as in Section 4, follow a model by Legler [31] which assumes the physical picture mentioned above. If  $\xi$  is the distance travelled by an electron from the last ionising collision the ionisation probability will be given by  $a(\xi) d\xi$  where  $a(\xi)$  is zero for  $\xi < x_0$  and will increase for  $\xi > x_0$ . In the same manner the attachment coefficient will depend on  $\xi$  and we replace the constant attachment coefficient  $\eta$



by  $e(\xi)$ . Starting with a single electron at  $x=0$ , the average number of avalanche electrons at a distance  $x$  that had the last ionising collision at a distance between  $\xi$  and  $\xi+d\xi$  from  $x$  is given by [31]

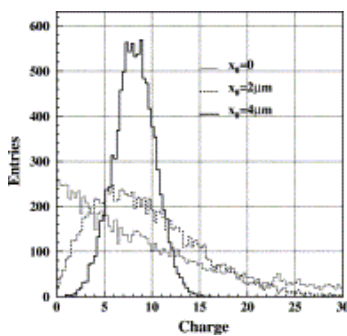
$$n(x, \xi) = A e^{-\lambda x} e^{-\int_0^\xi [a(\xi') + e(\xi')] d\xi'} \quad (56)$$

with boundary condition

$$n(x, 0) = 2 \int_0^\infty a(\xi) n(x, \xi) d\xi. \quad (57)$$

The parameter  $\lambda$  is defined by the boundary condition and  $A$  is a normalisation constant. This equation is the pendant to Eq. (3). We see that the average number of electrons increases exponentially for any given function  $a(\xi)$  and  $e(\xi)$ .

The equation determining the statistical fluctuation for this model is difficult to solve and we just show Monte Carlo results for different parameters. As a simple model we assume the function  $a(\xi)$  to be zero for  $\xi < x_0$  and  $a(\xi) = a_0$  for  $\xi > x_0$  and assume  $e(\xi) = \eta$  to be constant. Fig. 12 shows an example for a single electron avalanche spectrum for  $\alpha = 123/\text{mm}$ ,  $x_0 = 0, 2, 4 \mu\text{m}$ . For large  $x_0$  values the charge spectrum shows a pronounced peak.



Download: [Download full-size image](#)

Fig. 12. Charge distributions for avalanches started by a single electron and multiplying over a fixed distance of  $300 \mu\text{m}$  for  $\alpha = 123/\text{mm}$  and  $x_0 = 0, 2, 4 \mu\text{m}$ . For  $x_0$  values approaching  $1/\alpha = 8.13 \mu\text{m}$  the charge spectrum shows a pronounced peak.

This avalanche statistics effect has however a very small influence on the charge spectrum of the 0.3 and 2 mm RPCs since the position fluctuations of the primary electrons completely dominate the avalanche fluctuation as shown in the next section. For these types of RPCs the fluctuation model described in Section 4 is therefore perfectly applicable.

## 11. Monte Carlo and comparison with experiment

Finally, we want to compare the simulation procedure and detector physics parameters, outlined in the previous sections, to experimental results. The simulation procedure for a single event is the following

- The gas gap of size  $d$  is divided into  $N_{\text{step}}$  steps of size  $\Delta x = d/N_{\text{step}}$  corresponding to time steps of  $\Delta t = \Delta x/v$ , where  $v$  is the electron drift velocity from Fig. 7 at the given field.
- Primary clusters are distributed along the gas gap at distances following an exponential distribution with the mean taken from Fig. 3a.
- Primary electrons are put to each cluster following the cluster size distribution from

Fig. 3b.

- The avalanche for each single electron is simulated using  $\alpha$ ,  $\eta$ , and the procedure outlined in Section 4 with numbers for Townsend and attachment coefficient from Fig. 4. This provides  $N(t)$ , the number of electrons at time  $t$ .
- If  $N(t)$  exceeds a specified value  $N_{\text{sat}}$  the avalanche growth is stopped and the  $N_{\text{sat}}$  electrons propagate to the gap end. This procedure simulates the space-charge effect.
- The induced current signal is then calculated with Eq. (19) where the electron drift velocity is from Fig. 7 and the weighting field is from Eq. (21).
- In each simulation step the electrons are propagated by  $\Delta x(\Delta t)$ , the electrons leaving the gas gap are subtracted from  $N(t)$ , so the total signal has a maximum duration of  $T \leq d/v$ .

Since the drift velocity  $v$  is a function of  $E/N$  ( $N$  is the particle density), since the ‘reduced’ Townsend coefficient  $\alpha/N$  and attachment coefficient  $\eta/N$  are functions of  $E/N$ , and since the average distance between clusters  $\lambda$  scales with  $1/N$ , the gas properties given in Fig. 3, Fig. 4, Fig. 7 have to be scaled for pressures and temperatures different from **1023 mbar** and **396.15 K**. All the presented experimental measurements were performed at CERN with an average air pressure of around **970 mbar**.

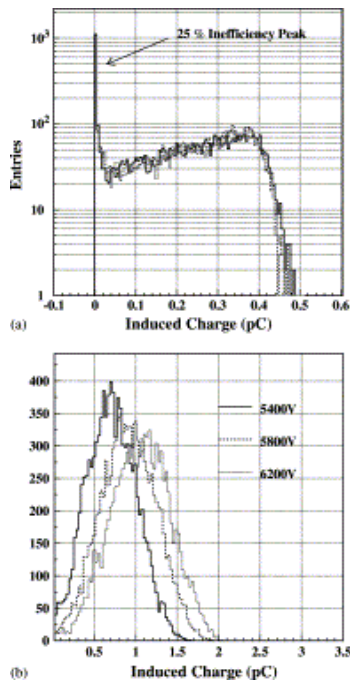
We include the electronics by convoluting the RPC signal with the amplifier delta response  $f(t)$

$$\begin{aligned} \mathbf{h}(\mathbf{s}) &= \mathbf{n}^{-n} \mathbf{e}^{\mathbf{n}} \mathbf{n}! \tau (1 + s\tau)^{n+1} \rightarrow \\ \mathbf{f}(t) &= \mathbf{L}^{-1}[\mathbf{h}(\mathbf{s})] = \mathbf{n}^{-n} \mathbf{e}^{\mathbf{n}} t \tau^n \mathbf{e}^{-t/\tau} \end{aligned} \quad (58)$$

where  $t_p = n\tau$  is the peaking time and  $n$  corresponds to the number of stages. The noise is included by adding Gaussian numbers to the signal in each time bin with a  $\sigma$  giving the correct Equivalent Noise Charge (ENC) at the output.

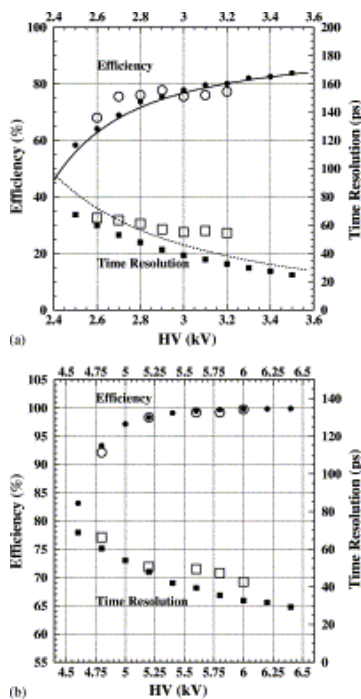
## 11.1. Timing RPCs

Fig. 13(a) shows a simulated charge spectrum for geometry from Fig. 1(c) at **3 kV** ( $E=100 \text{ kV/cm}$ ). First of all, the shape of the spectrum and the 25% inefficiency match quite well the numbers reported in [38], [22]. Overlaid is a simulation taking into account the high field avalanche statistics effect from the previous section. Although the charge spectrum for an electron multiplying over a fixed distance is strongly affected by the value of  $x_0$  (Fig. 12), the RPC spectrum shows no effect whatsoever, which is due to the fact that the charge fluctuations due to the primary ionisation positions are much larger. The charge spectra for three different voltages for the quad-gap RPC from Fig. 1b are shown in Fig. 13(b). The spectra are equal to the 4 times self-convoluted charge spectrum from the single gap RPC and resemble quite well the ones presented in Ref. [21]. Fig. 14 shows efficiency and time resolution versus voltage for single and quad gap RPC. The single gap RPC was simulated for the geometry from Fig. 1(c) giving a weighting field of 1.25/mm with **7 GeV** pions, i.e. 9.13 clusters/mm, **20 fC** threshold, **200 ps** amplifier peaking time, **1 fC** noise and Townsend coefficient, attachment coefficient and drift velocity for the gas  $\text{C}_2\text{F}_4\text{H}_2/\text{i-C}_4\text{H}_{10}/\text{SF}_6$  85/5/10 at **970 mbar**. The overlaid data are from Ref. [38].



[Download: Download full-size image](#)

Fig. 13. (a) Charge spectra for the single gap timing RPC assuming saturation at  $N_{\text{sat}}=1.6 \times 10^7$  electrons. The inefficiency is 25% for a 20 fC threshold. Three histograms for  $x_0=0, 2.5$  and  $5 \mu\text{m}$  are overlaid and show essentially no difference. (b) Charge spectra for the quad gap timing RPC assuming Townsend and attachment coefficients from Fig. 4. The avalanche in each gap is saturated at  $N_{\text{sat}}=1.6 \times 10^7$  electrons.



[Download: Download full-size image](#)

Fig. 14. Results for efficiency and amplitude corrected time resolution for the single gap (a) and quad gap RPC (b) for the parameters mentioned in the text at  $T=296.15\text{K}$  and  $P=970\text{mbar}$ . The open symbols are measurements. For the single gap RPC the formulas for time resolution and efficiency from , are overlaid.

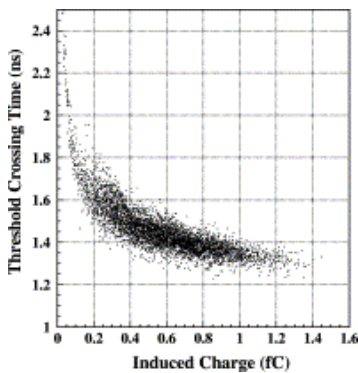
The simulation for the quad gap RPC was done with the same parameters, except for the weighting field (b) with 1.026/mm and an amplifier peaking time of **3 ns**. The overlaid data are from Ref. [20]. The agreement between measurements and simulation is quite acceptable. Fig. 15 shows the charge–time correlation for the quad gap RPC. Finally we want to compare the signal rise time to measurements. The induced current signal rises as  $\exp(f_0 t)$  where  $f_0 = (\alpha - \eta)v$ . In Ref. [39], the authors show that sending this signal through a general linear network, the output signal shows the same exponential rise and  $f_0$  can be measured by setting two thresholds to the signal. From the two threshold crossing times  $t_1$  and  $t_2$  one finds  $f_0$  by

$$\ln(\text{thr}_2/\text{thr}_1) = (t_2 - t_1)f_0. \quad (59)$$

This relation holds only if the input signal is ‘still’ and exponential at the threshold crossing times. We assume a ‘typical’ RPC signal for the geometry of Fig. 1a ( $E_w/V_w = 1.48/\text{mm}$ ), i.e. starting a single electron avalanche at a distance  $\lambda$  from the gas gap edge and saturating the signal at  $N_{\text{sat}} = 1.6 \times 10^7$  electrons

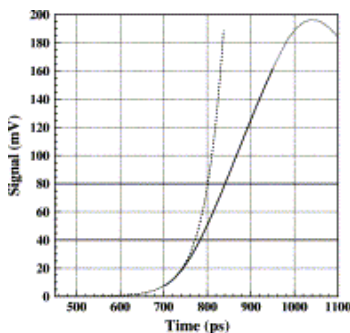
$$i(t) = E_w V_w e_0 v e^{(\alpha - \eta)vt}, t < t_{\text{sat}}, E_w V_w e_0 v N_{\text{sat}}, t_{\text{sat}} < t < T, t > T \quad (60)$$

where  $t_{\text{sat}} = \ln N_{\text{sat}} / (\alpha - \eta)v$  is the time when the avalanche goes into saturation and  $T = (d - \lambda) / v$  is the time when the electrons hit the gap edge. For the typical values from Eq. (25) we find  $t_{\text{sat}} = 702 \text{ ps}$  and  $T = 952 \text{ ps}$  and an induced charge of **0.23 pC**. For a preamp with  $t_p = 200 \text{ ps}$ , **1 mV/fC** sensitivity and two stages ( $n = 2$  from Eq. (59)) we find the preamp output signal shown in Fig. 16. For thresholds larger than **8 fC**, the threshold crossing times are larger than  $t_{\text{sat}}$  and Eq. (60) does not yield  $f_0 = (\alpha - \eta)v$ . For an operating voltage of **3 kV**, the full Monte Carlo gives an average value of  $f_0 = 11.6 \text{ GHz}$  for  $\text{thr}_1, \text{thr}_2 = 40, 80 \text{ fC}$  while  $(\alpha - \eta)v = 23.5 \text{ GHz}$ . This value is very sensitive to the amplifier bandwidth and the ‘real’ space-charge effect. Considering these uncertainties we consider the measured value of  $f_0 = 8.9 \text{ GHz}$  quoted in Ref. [39] to be ‘not too far’ from the simulation.



[Download: Download full-size image](#)

Fig. 15. Charge to time correlation for the quad gap RPC at **5200 V**.

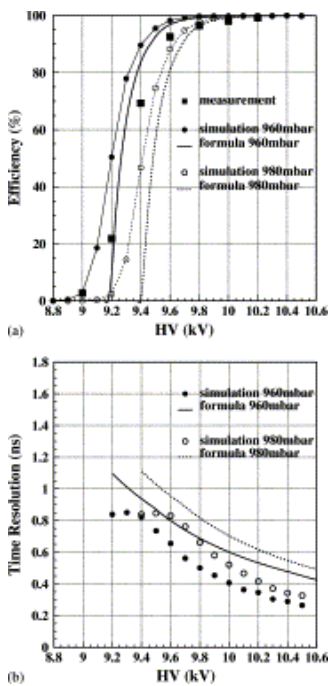


[Download: Download full-size image](#)

Fig. 16. Typical RPC signal for the timing RPC from Fig. 1a. At a threshold  $>8\text{fC}$  the signal does not rise exponentially.

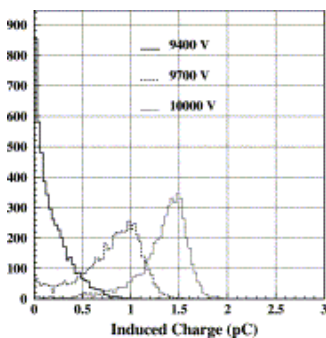
## 11.2. Trigger RPCs

Fig. 17a shows simulated efficiency and time resolution for the RPC from Fig. 2 and the gas  $\text{C}_2\text{F}_4\text{H}_2/\text{i-C}_4\text{H}_{10}/\text{SF}_6$  96.7/3/0.3. For  $\epsilon_r=10$  the weighting field is  $0.417/\text{mm}$ . A  $120\text{GeV}$  muon leaves  $9.64$  clusters/mm at normal conditions. The induced charge is divided by 2, accounting for the termination of the RPC strips and a  $100\text{fC}$  threshold is applied. A preamp peaking time of  $1.3\text{ns}$  was assumed. The measurements from Ref. [40] are quite well reproduced by the simulation. The simulated spectra are again unaffected by realistic  $x_0$  parameters. For  $N_{\text{sat}}=5\times 10^7$  electrons the spectra show the pronounced peak as observed in measurements (Fig. 18).



[Download: Download full-size image](#)

Fig. 17. Simulated trigger RPC efficiency (a) and time resolution (b) for  $T=296.15\text{K}$  and  $P=960/980\text{mbar}$  together with measurements from Ref. [40].



[Download: Download full-size image](#)

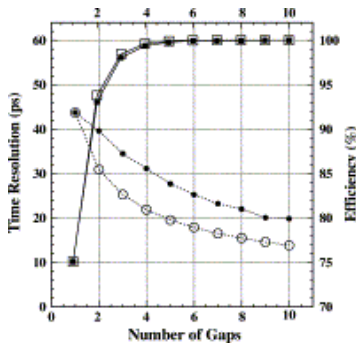
Fig. 18. Charge spectra of the trigger RPC for saturation at  $N_{\text{sat}}=5\times 10^7$  electrons.

## 12. Effect of number of gaps

In this section we want to investigate the effect of different numbers of gaps on time resolution and efficiency. The weighting fields for an RPC with  $n$  gas gaps of size  $d$  separated by  $n-1$  glass plates of thickness  $b$  and permittivity  $\epsilon$  is (Eq. (20)) [11]

$$\mathbf{E}_w \mathbf{V}_w = \epsilon n d \epsilon + (n-1)b, n > 1. \quad (61)$$

For the single gap RPC ( $n=1$ ) we use the geometry from Fig. 1a with corresponding weighting field from Eq. (21a). Since the weighting field decreases with the number of gaps the total induced charge is almost independent of the gap number [42], [3]. We assume an applied voltage that gives a field of **100 kV/cm** in the gas gaps, i.e. **3 kV** for single gap RPC, **6 kV** for double gap RPC, etc. Fig. 19 shows the time resolution and efficiency versus gap number. The figure also shows the  $1/n$  scaling of the single gap time resolution and  $1-(1-\epsilon)^n$  scaling of the single gap efficiency. We see that the efficiency follows the simple scaling considerations, the time resolution improvement however is less than one expects from naive scaling. The reason is that the timing is dominated by the gap with the largest signal. The largest signal gives the earliest threshold crossing time, so the timing of the multi-gap RPC is approximately given by the ‘earliest gap’. The earliest of  $n$  time measurements however has a larger r.m.s. than the average of  $n$  time measurements.

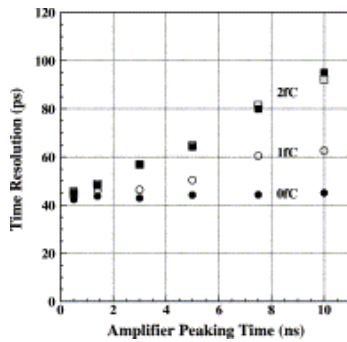


[Download: Download full-size image](#)

Fig. 19. Efficiency (black squares) and amplitude corrected time resolution (black circles) versus number of gas gaps. The open symbols give the numbers that are expected from naive scaling.

## 13. Amplifier bandwidth and noise

In this section we study the dependence of the RPC time resolution on the amplifier bandwidth. We characterise the amplifier by its peaking time  $t_p$  and order  $n$  as given in Eq. (59). We use the **300  $\mu\text{m}$**  single gap timing RPC at **3 kV** as an example. Fig. 20 shows the time resolution versus amplifier peaking time. Neglecting the noise, the time resolution is independent of peaking time since using the charge–time correlation one can fully correct for the introduced time slewing effects. Including the noise however shows that for slow amplifiers the intrinsic time resolution cannot be recovered. The reason is that the time jitter due to the noise (which cannot be corrected) increases for slower signal rise time.



[Download: Download full-size image](#)

Fig. 20. Simulation of the amplitude corrected time resolution versus amplifier peaking time for the **300  $\mu\text{m}$**  single gap RPC with a threshold of **20 fC** and Equivalent Noise Charge of 0, 1 and **2 fC**. Electronics noise introduces a jitter that cannot be recuperated by performing the amplitude correction. The influence of the noise therefore increases with the amplifier peaking time. For the **2 fC** curve, the results for two different noise spectra are shown.

## 14. Conclusions

We have presented an RPC simulation procedure including all detector physics and electronics effects from primary ionisation up to the frontend electronics output. Assuming a very prominent space-charge effect that is modelled by simply stopping the avalanche growth at a certain number of electrons, we can reproduce the observed RPC performance numbers quite well without any additional assumptions. We only assume physical parameters as given by Heed [17], Magboltz [18] and Imonte [19]. The outlined simulation procedure can be implemented in a Monte Carlo program in a very simple way. Generally we can conclude that

- Neglecting space-charge effects, the calculated average avalanche charges for the **300  $\mu\text{m}$**  timing RPCs are a factor  $10^7$  larger than the measured ones. This shows that space-charge effect play a significant role in RPCs [16].
- The RPC efficiency is approximately given by  $1 - e^{-(1-\eta/\alpha)d/\lambda} [1 + (V_w/E_w)(\alpha-\eta)/e_0 Q_t]^{1/\alpha\lambda}$ . It depends explicitly on the attachment coefficient and not just on the effective Townsend coefficient.
- The RPC time resolution is approximately given by  $\sigma_t = 1.28/(\alpha-\eta)v$  and is independent of the applied threshold.
- The high efficiency (75%) of single gap RPCs with **300  $\mu\text{m}$**  gas gap is explained by the large primary ionisation density (9.5/mm) of the tetrafluoroethane gas together with a very large effective Townsend coefficient of about 113/mm.
- Secondary particles produced in the RPC material should not play an important role in the RPC behaviour.
- The time resolution for an  $n$  gap RPC does not scale with  $\sigma_t/n$  where  $\sigma_t$  is the single gap RPC time resolution. The efficiency however does scale with the expected scaling law of  $1 - (1-\varepsilon)^n$  where  $\varepsilon$  is the efficiency of the single gap RPC.

- Neglecting electronics noise, the amplifier bandwidth has very little influence on the time




neglecting electronics noise, the amplifier bandwidth has very little influence on the time resolution since the time slewing introduced by slow amplifiers can be fully corrected by the charge–time correlation. Electronics noise however introduces a jitter at the threshold level which has more effect for slow amplifiers and the intrinsic time resolution cannot be recuperated.

## Acknowledgements

We thank Paulo Fonte for many interesting discussions.

[Special issue articles](#)   [Recommended articles](#)

## References

- [1] R. Santonico, R. Cardarelli  
Nucl. Instr. and Meth., 187 (1981), p. 377  
 [View PDF](#)   [View article](#)   [View in Scopus](#) ↗
- [2] R. Santonico, R. Cardarelli  
Nucl. Instr. and Meth., 263 (1988), p. 20
- [3] E. Cerron Zeballos, et al., A new type of resistive plate chamber: the multigap RFC, CERN PPE/95-166, 1995.  
[Google Scholar](#) ↗
- [4] W. Riegler, Induced signals in resistive plate chambers, CERN-EP-200J2-024, March 2002, Nucl. Instr. and Meth. A, in press.  
[Google Scholar](#) ↗
- [5] W. Riegler, D. Burgarth  
Nucl. Instr. and Meth. A, 481 (2001), p. 130
- [6] ICRU Report 31.  
[Google Scholar](#) ↗
- [7] H. Räther  
Electron Avalanches and Breakdown in Gases, Butterworth & Co, London (1964)  
[Google Scholar](#) ↗
- [8] F. Sauli, Principles of operation of multiwire proportional and drift chambers, CERN-77-09, CERN, 1977.  
[Google Scholar](#) ↗
- [9] W. Blum, L. Rolandi, Particle Detection with Drift Chambers, Springer, Berlin, 1993, ISBN 3-540-56425-X.  
[Google Scholar](#) ↗
- [10] E. Cerron Zeballos, *et al.*  
Nucl. Instr. and Meth. A, 381 (1996), p. 569

 [View PDF](#) [View article](#) [View in Scopus](#) ↗

[11] M. Abbrescia, *et al.*

Nucl. Instr. and Meth. A, 398 (1997), p. 173

 [View PDF](#) [View article](#) [View in Scopus](#) ↗

[12] M. Abbrescia, *et al.*

Nucl. Phys. B (Proc. Suppl.), 78 (1999), p. 459

 [View PDF](#) [View article](#) [View in Scopus](#) ↗

[13] P. Fonte

Nucl. Instr. and Meth. A, 456 (2000), p. 6

 [View PDF](#) [View article](#) [View in Scopus](#) ↗

[14] Discussions at the Sixth Workshop on Resistive Plate Chambers and Related Detectors, Coimbra, November, 2001.

[Google Scholar](#) ↗

[15] E. Cerron Zeballos, *et al.*

Nucl. Instr. and Meth. A, 396 (1997), p. 93

 [View PDF](#) [View article](#) [View in Scopus](#) ↗

[16] C. Lippmann, W. Riegler, Space charge effects and induced signals in resistive plate chambers, VI International Workshop on Resistive Plate Chambers and Related Detectors, Coimbra, November, 2001.

[Google Scholar](#) ↗

[17] I. Smirnov, Heed, program to compute energy loss of fast particles in gases, Version 1.01, CERN.

[Google Scholar](#) ↗

[18] S. Biagi, Magboltz, program to compute gas transport parameters, Version 2.2, CERN.

[Google Scholar](#) ↗

[19] S. Biagi, Imonte, program to compute gas properties, Version 4.5.

[Google Scholar](#) ↗

[20] P. Fonte, *et al.*

Nucl. Instr. and Meth. A, 449 (2000), p. 295

 [View PDF](#) [View article](#) [View in Scopus](#) ↗

[21] A. Akindinov, P. Fonte, *et al.*, A four-gap glass-RPC time-of-flight array with **90 ps** time resolution, CERN-EP 99-166, October 1999.


[Google Scholar](#) ↗

[22] P. Fonte, V. Peskov, High-Resolution TOF with RPCs, preprint LIP/00-04, October 2000.

[Google Scholar](#) ↗

[23] ALICE Collaboration, Addendum to the Technical Design Report of the Time of Flight System (TOF), ALICE-TDR-8-ADD-I, CERN-LHCC-2002-016, CERN, 24 April 2002.

[Google Scholar](#) ↗

- [24] R. Santonico, R. Cardarelli  
Nucl. Instr. and Meth. A, 263 (1981)
- [25] ATLAS Muon Spectrometer, Technical Design Report, CERN-LHCC-97-22, ATLAS TDR 10, CERN 1997.  
[Google Scholar ↗](#)
- [26] R. Camarri, *et al.*  
Nucl. Instr. and Meth. A, 414 (1998), p. 317  
[View in Scopus ↗](#)
- [27] F. Rieke, W. Prepejchal  
Phys. Rev. A, 6 (1972), p. 1507  
[View in Scopus ↗](#)
- [28] W. Riegler, *et al.*  
Nucl. Instr. and Meth. A, 443 (2000), p. 156  
 [View PDF](#) [View article](#) [View in Scopus ↗](#)
- [29] A. Fasso, *et al.*, FLUKA 99, Particle Transport Code, Version 1999.  
[Google Scholar ↗](#)
- [30] Helmut Vincke, CERN, private communication.  
[Google Scholar ↗](#)
- [31] Werner Legler  
Z. Naturforschung., 16a (1961), p. 253  
[Crossref ↗](#) [View in Scopus ↗](#)
- [32] J. Byrne, Proc. Roy. Soc. Edinburgh XVI A (1962) 33.  
[Google Scholar ↗](#)
- [33] Eduardo Gorini, Measurements of drift velocity and amplification coefficient in C<sub>2</sub>H<sub>2</sub>F<sub>4</sub>–Isobutane mixtures for avalanche operated RPC, Sixth International Workshop on Resistive Plate Chambers and Related Detectors, Napoli, October 1997.  
[Google Scholar ↗](#)
- [34] V. Golovatyuk, Laser beam studies of RPC behaviour in avalanche mode, Sixth International Workshop on Resistive Plate Chambers and Related Detectors, Coimbra, November, 2001.  
[Google Scholar ↗](#)
- [35] S. Ramo  
Proc. IRE, 27 (1939), p. 584  
[View in Scopus ↗](#)
- [36] R. Santonico, Avalanche growth in RPC's, Third International Workshop on Resistive Plate Chambers and Related Detectors, Pavia, October 1995.  
[Google Scholar ↗](#)
- [37] A. Manguarotti, A. Gobbi

Nucl. Instr. and Meth. A, 482 (2002), p. 192

- [38] P. Fonte, Development of large area and of position sensitive timing RPCs, Presentation at the Ninth Vienna Conference on Instrumentation Vienna/Austria, February 19–23, 2001.

[Google Scholar](#) ↗

- [39] A. Blanco, *et al.*  
Trans. Nucl. Sci., 48 (4) (2001)

- [40] G. Aielli, *et al.*  
Nucl. Instr. and Meth. A, 456 (2000), p. 77

 [View PDF](#) [View article](#) [View in Scopus](#) ↗

- [41] H. Genz  
Nucl. Instr. and Meth. A, 112 (1973), p. 83

 [View PDF](#) [View article](#) [View in Scopus](#) ↗

- [42] R. Santonico, RFC: present state of the art, VI International Workshop on Resistive Plate Chambers and Related Detectors, Napoli, October 1997.

[Google Scholar](#) ↗

---

Cited by (98)

### Particle identification

2012, Nuclear Instruments and Methods in Physics Research, Section A: Accelerators, Spectrometers, Detectors and Associated Equipment

*Citation Excerpt :*

...The physics of avalanches in RPCs is very complex, even though the simple geometry of the device would not suggest so. During the development of large area RPC systems for the LHC experiments, the detector physics of RPCs was therefore studied in detail [42–49]. The good detection efficiency of (single gap) RPCs is explained by the very large gas gain....

[Show abstract](#) ✓

### The HARP resistive plate chambers: Characteristics and physics performance

2007, Nuclear Instruments and Methods in Physics Research, Section A: Accelerators, Spectrometers, Detectors and Associated Equipment

[Show abstract](#) ✓

### An electron-multiplying 'Micromegas' grid made in silicon wafer post-processing technology

2006, Nuclear Instruments and Methods in Physics Research, Section A: Accelerators, Spectrometers, Detectors and Associated Equipment

[Show abstract](#) ✓

### Modeling of ionization produced by fast charged particles in gases

2005, Nuclear Instruments and Methods in Physics Research, Section A: Accelerators, Spectrometers, Detectors and Associated Equipment

[Show abstract](#) 

### [Detection of single electrons by means of a Micromegas-covered MediPix2 pixel CMOS readout circuit](#)

2005, Nuclear Instruments and Methods in Physics Research, Section A: Accelerators, Spectrometers, Detectors and Associated Equipment

[Show abstract](#) 

### [Space charge effects in Resistive Plate Chambers](#)

2004, Nuclear Instruments and Methods in Physics Research, Section A: Accelerators, Spectrometers, Detectors and Associated Equipment

[Show abstract](#) 



[View all citing articles on Scopus](#) 

[View Abstract](#)

Copyright © 2003 Elsevier Science B.V. All rights reserved.



All content on this site: Copyright © 2024 Elsevier B.V., its licensors, and contributors. All rights are reserved, including those for text and data mining, AI training, and similar technologies. For all open access content, the Creative Commons licensing terms apply.

